Mechanosensitive Membrane Channels in Action

Serge Yefimov,* Erik van der Giessen,* Patrick R. Onck,* and Siewert J. Marrink†
*Zernike Institute for Advanced Materials, Department of Applied Physics, and †Groningen Biomolecular Sciences and Biotechnology Institute, Department of Biophysical Chemistry, University of Groningen, Nijenborgh, Groningen, The Netherlands

ABSTRACT The tension-driven gating process of MscL from *Mycobacterium tuberculosis*, Tb-MscL, has been addressed at near-atomic detail using coarse-grained molecular dynamics simulations. To perform the simulations, a novel coarse-grained peptide model based on a thermodynamic parameterization of the amino-acid side chains has been applied. Both the wild-type Tb-MscL and its gain-of-function mutant V21D embedded in a solvated lipid bilayer have been studied. To mimic hypoosmotic shock conditions, simulations were performed at increasing levels of membrane tension approaching the rupture threshold of the lipid bilayer. Both the wild-type and the mutant channel are found to undergo significant conformational changes in accordance with an irislike expansion mechanism, reaching a conducting state on a microsecond timescale. The most pronounced expansion of the pore has been observed for the V21D mutant, which is consistent with the experimentally shown gain-of-function phenotype of the V21D mutant.

INTRODUCTION

Mechanosensitive (MS) channels are integral membrane proteins found in living cells, which are able to sense mechanical force and transduce it into an electrochemical signal. In nature, MS channels play an important role in various physiological processes like touch, hearing, and osmoregulation (1). During hypoosmotic shock in bacteria for instance, MS channels act as safety valves. Sensing the growing turgor pressure in the cell, they start to gate by opening a pore, thus reducing the turgor pressure and ultimately preventing the cell from lysis.

The class of prokaryotic MS channels consists of three families recognized in *Escherichia coli*, which are identified by their single MS channel conductance (1): MscM (≈0.5 nS), MscS (≈1 nS), and MscL (≈3 nS) for mini, small, and large conductance, respectively. By now, most attention in the literature has been confined to the MscL family, and the best-studied channel of the family is the MscL of *E. coli* (Eco-MscL) (2–7). It has been shown that Eco-MscL gates in response to membrane tension alone (7) by opening a large aqueous pore with a diameter up to 2–4 nm (8), as estimated by conductance measurements. Such a wide pore in the open state indicates that the channel undergoes significant conformational changes during the transition from closed to open state. The gating tension required for Eco-MscL is ~8–10 mN/m (7,9). Another remarkable property of the channel is that it fully retains its gating functionality when purified and reconstituted into lipid vesicles (10) and other synthetic membrane systems.

While Eco-MscL has been extensively characterized both in vivo and in vitro, the other representative of the MscL family, Tb-MscL, has received less attention. The gating tension for WT Tb-MscL is typically two-times higher (3) than that for Eco-MscL and approaches the rupture limit of normal lipid membranes, thus limiting the successful outcome of experiments on gating of Tb-MscL. However, recent experiments on site-directed mutagenesis have produced a number of gain-of-function (GOF) Tb-MscL mutants (3, 11,12), which do gate at tensions within the physiological range. The resolved three-dimensional crystal structure of Tb-MscL (13) in the closed state has become a significant step forward in the problem of understanding the gating mechanism of MscL. At this point, molecular modeling approaches (e.g., (14–17)) become applicable to the problem, using the crystal structure of Tb-MscL as a starting point. A major goal of the molecular simulations is to predict the channel structure in the open state and its gating mechanism, both of which are as yet undisclosed and are subject to ongoing debate (6,18,19).

It has not been possible so far to directly simulate the gating mechanism of MscL in atomic detail by means of molecular dynamics (MD). Modeling of patch-clamp experiments on systems with a single MscL embedded in a lipid bilayer has been attempted by several authors (14–16), but the timescales reached were many orders-of-magnitude shorter than physiological ones. The timescales affordable by such all-atom models hardly exceed 10 ns, whereas the MscL activity takes place on timescales of milliseconds up to seconds. To overcome this enormous gap between experimental and simulation timescales, either unphysiological high tension conditions (15) or biasing techniques like steered (17) or targeted (20) MD, have to be applied. There have also been attempts to model MscL gating using continuum descriptions, either addressed analytically (21,22) or, more recently, numerically by a finite element method (23). Although these models can treat large length- and timescale processes providing valuable qualitative insight into the problem, they lack

---

Submitted August 16, 2007, and accepted for publication October 22, 2007.

Address reprint requests to Erik van der Giessen, E-mail: e.van.der.giessen@rug.nl.

Editor: Helmut Grubmuller.

0006-3495/08/04/2994/09 $2.00

doi: 10.1529/biophysj.107.119966

structural details which can be crucial in capturing the gating mechanism.

In this work, we take an alternative approach, and present a novel coarse-grained (CG) MD lipid-peptide model applied to the problem of the MscL gating. The proposed model is based on the CG MARTINI model for biomolecular systems recently developed by Marrink et al. (24,25). This model maps, on average, four heavy atoms onto a single coarse-grained bead, which interact via a Lennard-Jones (LJ) potential energy function. The underlying chemical nature of the beads is mimicked by the relative strength of the LJ interactions, which are parameterized against experimental data on partitioning free energies. Following a similar procedure, here the model has been extended with a CG representation of the protein structures and protein-lipid interactions. Partitioning data of key amino acids are reproduced to a satisfactory level (within 2 kT, see Methods).

The goal of the article is to reveal the details of the tension-driven gating of Tb-MscL, using a protein model at near-atomic detail in an explicit membrane/water environment. We present results from multi-microsecond simulations of both WT Tb-MscL (WT in the remainder of the article) and its GOF mutant V21D embedded in a DOPE bilayer. Note that whereas experimentally pure DOPE systems do not form bilayers, within the simulation box DOPE bilayers are stable due to the periodic boundary conditions used. Preliminary results obtained with other lipid components indicate qualitatively similar gating behavior. Detailed comparison of the gating behavior in membranes of different lipid compositions will be the topic of a future publication. Here we will show that both the WT and the mutant are able to sense the applied tension and, in accordance with the experimental observations, have different gating thresholds due to the performed mutation. We will also present key structural features of the channels during the gating, which is akin to the irislike pathway proposed by Sukharev et al. (18).

METHODS

Basic CG parameters

The basic parameters for the combined peptide-lipid force field are the same as used for the lipid force field described previously (24). It uses a four-to-one mapping, i.e., on average four heavy atoms are represented by a single interaction center. Currently the model considers four main types of interaction sites only: polar (P); nonpolar (N); apolar (C); and charged (Q). For particles of type N and Q, four subtypes (0, *d*, *a*, and *da*) are further distinguished. Subtype 0 applies to groups in which no hydrogen-bonding capabilities exist, *d* and *a* for groups that could act as a hydrogen-bond donor or acceptor, respectively, and *da* for groups with both donor and acceptor options. All nonbonded particles interact via a Lennard-Jones (LJ) potential. The strength of the interaction, determined by the value of the well-depth ε_{ij}, depends on particle types *i* and *j*. The value ranges from $\varepsilon = 5$ kJ/mol for interactions between polar groups to $\varepsilon = 1.8$ kJ/mol for interactions between polar and apolar groups mimicking the hydrophobic effect. The effective size of the particles is governed by the LJ parameter $\sigma = 0.47$ nm for all particle types. For reasons of computational efficiency a mass of $m = 72$ amu (corresponding to four water molecules) is assigned to each CG site. In addition to the LJ interaction, charged groups (type Q) interact via the normal electrostatic Coulombic potential applying a relative dielectric constant $\varepsilon_r = 20$ for explicit screening.

Bonded interactions between chemically connected sites are described by a weak harmonic potential with an equilibrium distance $R_{\text{bond}} = \sigma = 0.47$ nm, and a force constant of $K_{\text{bond}} = 1250$ kJ mol^{-1} nm^{-2}. To represent chain-stiffness, a weak harmonic potential is used for the angles with equilibrium bond angle $\theta_0 = 180°$, and a force constant of $K_{\text{angle}} = 25$ kJ mol^{-1} rad^{-2}. The double bond in DOPE is modeled using $\theta_0 = 120°$ and $K_{\text{angle}} = 35$ kJ mol^{-1} rad^{-2}. The area per lipid of pure DOPE bilayers, at low temperatures, compares well with the experimental value: 0.61 nm^2 at $T = 273$ K versus 0.65 nm^2 experimentally (26) at $T = 271$ K. At higher temperatures, DOPE readily converts into an inverted hexagonal phase, a process that is reproduced with the CG model (27). In the current simulation setup with excess solvent, however, the bilayer phase is stabilized by the periodic boundary conditions, at an area/lipid of 0.66 nm^2 at $T = 323$ K and zero surface tension. More details about the CG MARTINI model and its applications to model membranes can be found in the original articles (24,25).

Parameterization of MscL

Most amino acids were mapped onto single standard particle types in a similar way, as was done recently by us and other groups (28–30). The most apolar amino acids (Leu, Pro, Ile, and Val) were represented as C-type particles; intermediately polar amino acids were represented by N_{da} (Thr, Ser) or N_0 (Cys, Met), the polar uncharged amino acids by P (Asn, Gln); and the charged side chains as Q_d (Lys, Asp), Q_a (Glu), or Q_{da} (His). The larger Arg side chain was modeled by two particles (N_d-Q_{da}), and the bulkier ring-based side chains by three N_0-N_0-N_0 (Phe), N_0-N_0-N_{da} (Tyr), or C-C-N_d (Trp) CG particles. The Gly and Ala residues were only represented by the backbone particle, which is of type N_0 for all residues. Note that Tb-Mscl does not contain all amino acids. Table 1 lists the particle type assignment for the amino acids present in Tb-MscL.

The particle types for most amino acids were estimated from a comparison between simulation results and experimental measurements of the water/oil partitioning coefficients of the amino-acid side-chain analogs. The experimental values could be reproduced to within 2 kT, a level of accuracy hard to obtain even with fine-grained models. The remaining amino-acid particle type assignment was based on intuitive judgment of the relative hydrophilicity and hydrogen-bonding capacities of the underlying chemical structure. The partitioning behavior of the CG amino acids is also summarized in Table 1. Simulation data are obtained from equilibrium densities of low concentrations of CG beads dissolved in a water/butane two-phase system. The experimental data are taken from the literature (31,32) and refer to partitioning between water and cyclohexane. Both simulation and experimental data are obtained at 300 K.

TABLE 1 Partitioning free energies (in kJ/mol) between water and oil for side chains of amino acids present in Tb-MscL in the CG model compared to experimental data (31,32)

Residue	Bead type	ΔG^{CG}	ΔG^{EXP}
Leu	C	22	22
Ile	C	22	22
Val	C	22	17
Pro	C	22	—
Thr	N_{da}	−12	−11
Ser	N_{da}	−12	−14
Asn	P	−23	−28
Lys	Q_d	−23	—
Asp	Q_d	−23	—
Phe	N_0-N_0-N_0	19	17
Tyr	N_0-N_0-N_{da}	2	−2

Gly and Ala amino acids are represented by the backbone particle only.

The geometry of the amino acids is such as to mimic the underlying chemical structure as closely as possible. Unlike the lipid force field, for the peptide we allowed bond lengths to deviate from the standard value of 0.47 nm. The secondary structure of MscL was preserved using an additional set of constraints. To mimic hydrogen bonding between the N–H and C=O groups of every fifth residue of the secondary structure elements (thus, defining an ideal α-helix), harmonic distance restraints between the backbone particles of these residues were applied. The distance was maintained at 0.6 nm, with a force constant of $K_{\mathrm{bond}} = 12{,}500\ \mathrm{kJ\ mol^{-1}\ nm^{-2}}$.

The current setup has been tested on the behavior of small peptides with respect to membrane binding. It was found that the preferred binding mode (i.e., whether interfacially bound or in a TM orientation), for a series of α-helical peptides, could be well reproduced. Although this initial setup as well as similar ones (28–30) seem to behave quite realistically, a more thorough design and testing of the protein CG force field is currently underway and will be published elsewhere.

Simulation details

A CG structure for Tb-MscL has been obtained by converting the 3.5 Å crystal structure from PDB entry 1MSL (13) using the mapping procedure described in the previous subsection. The CG protein structure was then embedded in a preequilibrated CG DOPE bilayer in the liquid-crystalline phase and solvated with CG water molecules. This led to a system containing 1 MscL, 392 lipids, and 12,207 water molecules, giving a total of 18,790 atoms in a rectangular box. To simulate a system with the V21D mutant having a nonzero net charge, seven Na counterions were added to neutralize the system charge. Periodic boundary conditions were applied in all directions.

The simulations were performed using the GROMACS simulation package (33), Ver. 3.1.4. Analysis of the simulation trajectories and the MscL structures has been performed using various GROMACS tools. Profiles of the channel pore have been obtained in the HOLE program (34) using a spherical probe. The systems were simulated in the NPT ensemble using weak coupling schemes to temperature and pressure baths (35). To simulate the tension-induced gating of MscL, a semiisotropic pressure-coupling scheme leading to a constant lateral tension in the membrane has been used. To study the sensitivity of Tb-MscL gating to different levels of the membrane tension, we have performed several simulation sets with four values of constant negative lateral pressure, $P_{\|}$: −50, −80, −90, −95, and −100 bar at 323 K. $P_{\perp} = 1$ bar in the direction of the bilayer normal was kept in all simulations. The lateral tension in the bilayer is estimated as $\gamma = L_z(P_{\perp} - P_{\|})$ (36), where L_z is the actual time-averaged height of the simulation box. The rapid initial 0.5 μs opening stage, in which the bilayer shows the largest deformation, is omitted in the estimation of the tension. The tensions reported in this article are accurate within a margin of 1 mN/m. Before the simulations of MscL gating, the assembled systems with WT and V21D mutant have both been simulated for 120 ns with the protein atoms positionally restrained and then equilibrated unrestrained for 400 ns each at a constant temperature, $T = 323$ K, and zero surface-tension conditions (anisotropic pressure coupling with $P_{\|} = P_{\perp} = 1$ bar).

The integration time step of all the simulations was set to 80 fs. Note that this, and all other times reported in this article, is an effective time. The CG dynamics is faster than the all-atom dynamics because the CG interactions are much smoother compared to atomistic interactions. Based on comparison of diffusion constants in the CG model and in atomistic models, the effective time sampled using CG is three- to sixfold larger (24). When interpreting the simulation results with the CG model, a standard conversion factor of four is used, which is the effective speedup factor in the diffusion dynamics of CG water compared to real water. However, for protein systems, no explicit testing of the actual speedup due to the CG dynamics has been performed. Therefore, the timescale of the simulations has to be interpreted with care.

RESULTS AND DISCUSSION

MscL structure in the closed conformation

The structure of Tb-MscL is organized as a fivefold symmetric homopentamer (13). Each of the five subunits is formed by two TM (TM1 and TM2) and one cytoplasmic α-helices. In the closed state, the structure of the TM domain of Tb-MscL resembles a system of two truncated cones enclosed in each other. The TM1 helices, which are overall more hydrophilic, form the inner cone tapering toward the cytoplasm and line up at the channel pore, whereas the TM2 helices enriched in hydrophobic amino acids face the lipids and, thus, form the outer cone of almost a cylindrical shape. The structure of the TM domain of WT after equilibration in a tensionless DOPE bilayer at a reference temperature $T = 323$ K is given in Fig. 1.

The narrowest part of the WT channel pore, the so-called constriction region, is created by the residues Ile-14–Val-21 at the cytoplasmic end of the TM1 helix of all five subunits. The main characteristics of this region are dominating hydrophobicity of the residues facing the pore and a very narrow pore opening (≈0.2 nm in diameter). This allows us to speak about the region as of a hydrophobic lock, presumably forming the major energy barrier in the transition between the closed and open conformations.

The second channel that we have chosen to study is a site-directed Tb-MscL mutant (V21D) in which the key nonpolar residue Val-21 in the hydrophobic lock has been substituted with Asp that carries a hydrophilic acidic group. Experimentally this mutation gives rise to a more sensitive channel and lowers the gating threshold by a factor of two with re-

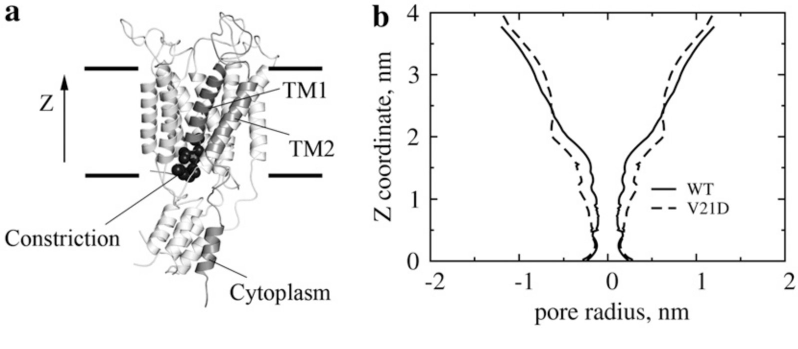

FIGURE 1 (*a*) Structure of the WT channel in the closed state after equilibration, side view; (*b*) pore profiles of WT and V21D mutant in the closed state after equilibration.

spect to WT (3). Pore profiles of the two channels in the closed state after equilibration are shown in Fig. 1 *b*. The pore around the constriction region in V21D shows some widening (≈10%) with respect to that in WT due to presence of Asp-21 residue. Another interesting observation is that the pore entry at the periplasmic surface in V21D is somewhat narrower than that in WT. For both WT and V21D it is found that the channel pore is partially hydrated in the region where it is lined primarily by the hydrophilic residues. This is apparent from Fig. 2 *a*, which shows the V21D embedded in the membrane, equilibrated in the closed state. Partial hydration is consistent with estimations made by Oakley et al. (37) that Tb-MscL in the closed state could be filled with water to a depth of around the average lipid monolayer thickness below the periplasmic surface. The channel at the constriction region remains occluded, as expected.

Fig. 2 *a* also reveals that the bilayer in close proximity to the protein adjusts its thickness to match the height of the TM domain of the channel. This effect, known as hydrophobic matching (1), has also been observed in an atomistic study of lipid-MscL interactions (38). The effect appears strongest at the cytoplasmic surface. The channel, in turn, also shows signs of such hydrophobic matching by changing the tilt of the helices in the TM domain with respect to the lipid bilayer normal. The tilt angle of ≈30°, obtained in the x-ray structure for both TM1 and TM2 helices, changes to ≈35° and ≈27° for TM1 and TM2, respectively. Consequently, in the closed structure the TM1 helices span both the lipid headgroup region and the hydrophobic core of the bilayer, while the TM2 ones penetrate only the hydrophobic region of the bilayer. This effect is also observed in the simulations with WT.

Tension-induced gating

To mimic the hypoosmotic gating of the channel we have performed a set of simulations in which the equilibrated systems were subjected to different levels of lateral tension during periods of several microseconds. The tension on the membrane was created by applying a negative pressure along the lateral directions (see Methods). The results of the constant tension simulations, performed at $T = 323$ K, are summarized in Fig. 3, *a* and *b*, which shows the time evolution of the minimum channel pore radius, r, measured at the constriction region for different levels of the applied tension γ. For a membrane tension of $\gamma \leq 60$ mN/m, no significant deviations from the starting (closed) conformation are observed in the pore structure, neither for the WT nor for the V21D. Application of higher tensions (73 mN/m), however, triggers a significant pore opening. Measured at the constriction zone, the pore widens from $r \approx 0.1$ nm in the closed state to ≈0.2 nm and ≈0.4 nm in the expanded state for WT and V21D channels, respectively. More pronounced openings of the pore at the constriction region ($r \approx 0.4$ nm for WT) and up to $r \approx 0.75$ nm for V21D are achieved in the simulations with $\gamma = 77$ mN/m. Further expansion of the pore in V21D is often accompanied by loss of a contact between the TM1 and TM2 helices of the adjacent subunits causing a disintegration of the TM structure.

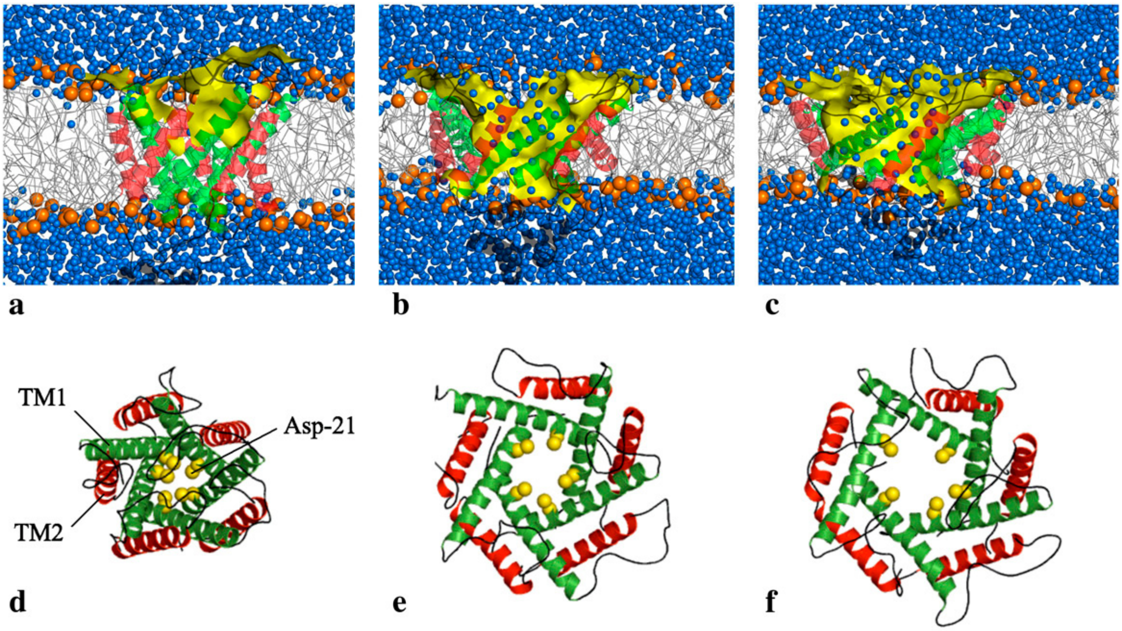

FIGURE 2 Time evolution of a system with V21D simulated at $\gamma = 77$ mN/m and $T = 323$ K. Side view snapshots are taken at (*a*) $t = 0$ μs, (*b*) $t = 0.5$ μs, and (*c*) $t = 5$ μs. Corresponding extracellular views of the TM domain at (*d*) $t = 0$ μs, (*e*) $t = 0.5$ μs, and (*f*) $t = 5$ μs are shown. Blue spheres denote water, orange spheres the phosphate site of the lipid headgroups, and gray lines are used to depict the lipid tails. The yellow surface represents the channel wall.

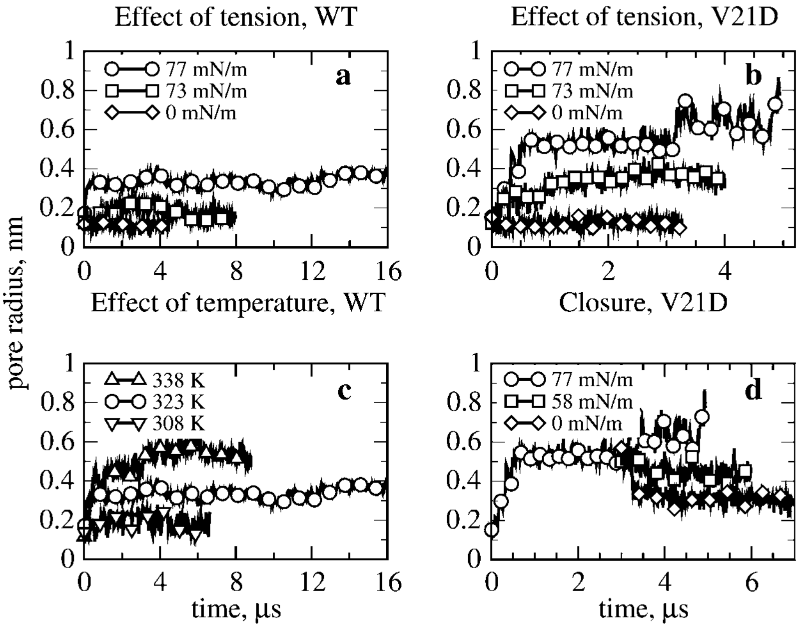

FIGURE 3 Time evolution of the minimum pore radius, *r*, at the constriction region at different levels of membrane tension. (*a*) Minimal opening of the WT channel, (*b*) substantial opening of the V21D channel, (*c*) opening of the WT channel at elevated temperature, and (*d*) reversible closure of the V21D channel at reduced tension levels.

Application of tensions exceeding 80 mN/m leads to rupture of the DOPE bilayer. Note that a tension of 80 mN/m is actually larger than a phospholipid membrane would be able to withstand in an experimental situation; rupture typically occurs around a few mN/m (39,40). However, pore formation preceding membrane rupture is a kinetic process and therefore depends on the loading rate of the applied tension (40). In MD simulations, the accessible timescale is limited to microseconds, corresponding to an effective loading rate much higher than observable in experiments. Consequently, pore formation at lower tensions does not occur. Atomistic simulations of lipid membranes reveal comparable rupture tensions on the nanosecond timescale (41). The same argument applies to the comparison of the observed gating tension ($\geq$ 60 mN/m) relative to the experimentally observed tension ($\gamma \geq 20$ mN/m for the WT and $\geq$10 mN/m for the V21D mutant examined in patches excised from giant *E. coli* spheroplasts (3)). The microsecond timescale accessible in the simulations is still much faster than the in situ gating time which is estimated to be in the millisecond regime (1). To probe gating on the microsecond timescale, higher tensions are therefore required.

To address the kinetic aspect of gating further, the reversibility of the gating process has been checked for the V21D mutant. The system simulated at $\gamma = 77$ mN/m (see Fig. 3 *d*) has been relaxed after 3 μs to the tension levels of 58 and 0 mN/m, respectively. Fig. 3 *d* shows that the system relaxation due to an instantaneous drop of the applied tension from 77 to 58 mN/m leads to a stable expanded state after a relatively minor initial closure of the channel pore from $r \approx$ 0.55 nm to $r \approx 0.45$ nm. Relaxation to a tension free state leads to an abrupt pore closure down to $r \approx 0.35$ nm with further closure to $r \leq 0.3$ nm in the next 4 μs. Complete sealing of the pore to $r \approx 0.1$ nm in the initial closed state has not been obtained on the accessible timescale.

Since the channel opening achieved for the WT is more limited compared to that of V21D, we have performed an additional set of simulations at an elevated temperature of 338 K aiming to accelerate the dynamics of the WT system. Indeed, these simulations show that a more expanded state ($r \approx 0.62$ nm, see Fig. 3 *c*) at the constriction region is reached at a lower tension of 72 mN/m and at a shorter timescale than in the reference case ($\gamma = 72$ mN/m is the maximum tension that the bilayer can sustain at 338 K). A simulation performed at $T = 308$ K has shown that at this temperature the lipid bilayer with more closely packed lipids becomes more resistant to the applied deformations and can sustain higher tensions (up to $\gamma = 90$ mN/m). However, even a high tension of 80–85 mN/m in the system was not able to trigger a pore opening in the constriction region with more than $r \approx 0.25$ nm (see Fig. 3 *c*).

In summary, the simulations of Tb-MscL embedded in a membrane under tension clearly show that the mutant gates much easier (i.e., at lower tensions) than the WT. This result is consistent with the GOF phenotype of the mutant shown experimentally (3). Extra expansion of the pore in V21D compared to WT is a direct consequence of the Coulombic repulsive interactions between the mutated sites at the TM1 helices. This apparently relaxes the hydrophobic lock in the constriction region and thus lowers its energy barrier toward the opening. Interestingly, in our simulations we observe gating of the channel at tensions just below the rupture strength of the bilayer. This is also observed for the experimental gating of the Tb-MscL channel (3).

Irislike gating pathway

Upon applied lateral tension above the gating threshold, both WT and V21D undergo the gating transition and follow qualitatively the same pathway. We now discuss the gating pathway of Tb-MscL based on the results obtained in the simulations with V21D mutant at $\gamma = 77$ mN/m and $T = 323$ K, as this system gives rise to the largest opening. Time evolution of this system is depicted in Fig. 2 in a set of snapshots.

To sustain the applied tension, the bilayer undergoes significant contraction within the first hundreds of nanoseconds in the direction of the *z* axis (the phosphate-phosphate distance decreases from 4.5 nm to 3.0 nm) and an isotropic expansion in the lateral plane (from an equilibrated area of 0.66 nm^2 per lipid headgroup to a maximum expanded area of 1.2 nm^2). The deformations in the bilayer trigger, in turn, major conformational changes of the MscL complex and give rise to its closed-to-open conformation transition that takes place on a much longer, microsecond timescale. Large-scale conformational changes are mainly seen in the TM domain (see Fig. 2). Fig. 2, *e* and *f*, shows that the opening of the pore lined up exclusively by all five TM1 helices in the closed state (Fig. 2 *d*), occurs due to rearrangements of the TM1 helices themselves. TM2 helices are not directly involved in the pore structure formation. The role of the outer TM2 helices in getting to the fully open state can be seen in protecting TM1 helices from the extensive contact with the lipids at all times and creating enough space for the spatial rearrangements of the TM1 helices. These rearrangements are favored by the large areal expansion in the bilayer. As for the cytoplasmic helices, they are found to be very flexible in their motions, and to remain in the solution even though moving somewhat closer to the bilayer (see Fig. 2, *a*–*c*) upon lateral expansion of the TM domain. They do not seem to affect the functionality of the channel.

Taking into account the main structural features of the channels during the transition, one can conclude that the gating mechanism seen in the simulations is similar to the one proposed in a theory of an irislike gating pathway (18). At the same time it is inconsistent with the structural models based on a 10-helix barrel-stave pore geometry (e.g., (44,45)), in the open state. Interestingly, the open channel is not completely symmetric. This is easily judged from inspection of the visual image (Fig. 2 *f*). Recent disulfide crosslinking experiments (42,43) point to a similar asymmetry during MscL gating.

We have to keep in mind, though, that the gating mechanism, as observed in our simulations, occurs under nonphysiological conditions. As discussed before, the tensions required for spontaneous gating on the microsecond timescale are large compared to in vitro or in vivo conditions. The extensive thinning of the membrane before gating is a direct consequence, putting a possible bias to our results. Nevertheless, the observed gating mechanism appears reasonable, and is in line with the majority opinion as expressed in the literature. Next, we will discuss the gating mechanism seen in the simulations in more detail.

Two-stage opening

The gating mechanism can be split into two main stages, in terms of the pore expansion rates (Fig. 3) measured at the constriction region. Both stages can be characterized by different dominating spatial rearrangements of the helices in the TM domain, which occur at different timescales. These complex spatial rearrangements of the TM helices can be split into three main modes: outward motions with respect to the fivefold symmetry axis (the *z* axis); rotations in the lateral plane; and tilts with respect to the *z* axis. The rearrangements of the helices give rise to an asymmetric expansion of the pore, as illustrated in Fig. 4 by means of the vertical pore profiles. The profiles are taken in the closed (C) state and at the end of the first and second stages marked with E_1 ($t = 0.5$ μs) and E_2 ($t = 5$ μs) states, respectively.

The first stage is characterized by a rapid expansion of the pore, which occurs at the same expansion rate for both channels (see Fig. 3, *a* and *b*) and takes up to 0.5 μs. At the end of this stage, the pore radius at the constriction region has increased up to 60–70% of its maximum value in the final expanded state obtained. Main contributions to the conformational changes in the TM domain structure arise from the tilt and outward motions of the TM1 and TM2 helices. The TM domain complies with the deformations in the bilayer and, therefore, undergoes significant flattening (Fig. 2 *b*) in

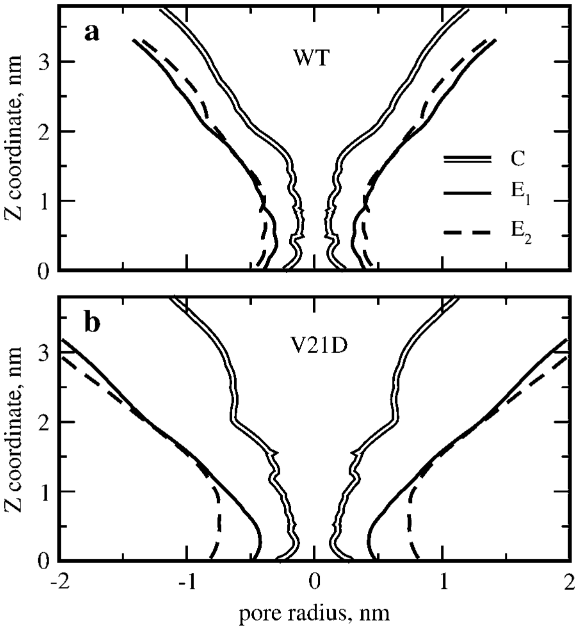

FIGURE 4 Pore structure profiles of closed (C) and two expanded states (E_1 at $t = 0.5$ μs and E_2 at $t = 5$ μs) at the end of each stage in the simulations at $T = 323$ K and $\gamma = 77$ mN/m in WT and V21D.

the projection of the z axis and radial expansion (Fig. 2 *e*) in the lateral plane. The flattening of the TM domain is associated with the tilt of the TM1 and TM2 helices up to 60° ± 5° and 50° ± 10° in V21D (50° ± 5° and 45° ± 10° in WT), respectively, at the end of the stage. Pivoting points of the TM1 helices are located inside the constriction region. This suggests that the tilt alone causes a noticeable widening of the pore entry at the periplasmic surface at the cost of a nearly rigid constriction (similar to a flower bud opening its petals). A similar effect of tilt only, which does not lead to the gating, has been observed in the simulations at $\gamma = 60$ mN/m.

Unlike the TM1 helices, the TM2 ones are found to have somewhat more freedom in tilt with larger and more frequent fluctuations than the TM1 helices. This is apparently due to extensive interactions with tails of the neighboring lipids and less constrained geometry, while TM1 helices, shielded by the TM2 ones from the lipid environment, exhibit more conservative and cooperative motions. The TM2 helices are also found to interact more with the TM1 ones of the adjacent subunit by having approximately the same lateral orientation (Fig. 2, *d–f*) and maintaining an average distance of ≈1.1 nm, rather than interacting with the TM1 helix of the same subunit. This, apparently, is the most efficient way to shield the internal pore from its exposure to the surrounding lipids.

Along with the tilt, a significant contribution to the lateral expansion of the periplasmic part of the channel comes from the outward motions of the C- and N-termini of the TM1 and TM2 helices, respectively, from the fivefold symmetry axis of the channel. The periplasmic ends of the TM1 and TM2 helices are seen to move outward cooperatively, keeping the average distance between them unchanged. The same conclusion holds for the cytoplasmic ends. This suggests that the interhelical interactions of the TM1 and TM2 helices are stronger that those between the TM2 ones and the lipid environment. Lateral expansion of the cytoplasmic part at this stage lacks tilt contribution and, therefore, is less pronounced. As a consequence, the tilt contribution to the lateral expansion of the periplasmic part together with the resistance toward opening of the constriction region results in an overall nonuniform expansion of the TM domain. This, in turn, leads to a more pronounced conical shape of the pore profile in the expanded state after the first stage (see E_1 states in Fig. 4).

The second stage ($t \geq 0.5$ μs) reveals that further widening of the pore occurs predominantly around the constriction region at a much lower expansion rate than that at the first stage. This widening is mainly due to the TM1 helices rotating in the lateral plane in anticlockwise direction (from the extracellular view). This effect follows from the observations that the tilt and lateral expansion in the periplasmic-part no longer progress significantly, while the cytoplasmic part of the channel keeps increasing its lateral area (Fig. 3), as is confirmed by the profiles of WT and V21D in their final expanded conformations (see E_2 states in Fig. 4). Evidently, the effect is much more pronounced in the mutated channel than in WT. Average outer dimensions of the TM domain of V21D in the final stable expanded state reach 6.5 and 5 nm in diameter with associated area changes of ≈11 nm^2 and ≈6.5 nm^2 at the periplasmic and cytoplasmic surfaces, respectively, compared to the closed conformation. This suggests that the conical shape of the TM domain obtained after the first stage is not an energetically favorable and stable one, but rather one representing an intermediate state along the gating pathway.

Channel functionality in the open state

To call the most expanded state observed in our simulations an open state, it is essential that a water channel is actually formed inside the channel. To estimate the hydration level of the pore, we have calculated the total number of water molecules that are found inside the pore (within a 3-nm-diameter sphere placed in the center of mass of the C_α beads of five TM1 helices), i.e., n^{pore}; and inside the constriction region (within a 1.4-nm-diameter sphere placed in the center of mass of the C_α beads forming the hydrophobic lock), i.e., n^{cr}.

The outcome of the calculations shows that the pore openings achieved in the simulations of the WT at 338 K and the V21D mutant at 323 K are large enough to result in the presence of a stable water-filled pore. The hydration level of the V21D pore is found to have increased from $n^{\mathrm{pore}} = 20$ and $n^{\mathrm{cr}} = 0$ water molecules in the closed state to $n^{\mathrm{pore}} = 55$ and $n^{\mathrm{cr}} = 10$ in the final expanded state (see Fig. 5). For the WT (at $T = 338$ K), the increase is from $n^{\mathrm{pore}} = 19$ and $n^{\mathrm{cr}} = 0$ to $n^{\mathrm{pore}} = 40$ and $n^{\mathrm{cr}} = 8$. At the lower temperature (323 K) the pore hydration level of the WT remains nearly unchanged with respect to the closed state at $n^{\mathrm{pore}} = 18$. Nevertheless, due to the obtained opening ($r \approx 0.4$ nm), the pore around the constriction region becomes transiently permeable to water, exhibiting flickering activity. Simulations at 308 K show no hydration of the constriction region at any recorded state.

The analysis of the hydration properties of the Tb-MscL channel allows us to call the final expanded state, both for the

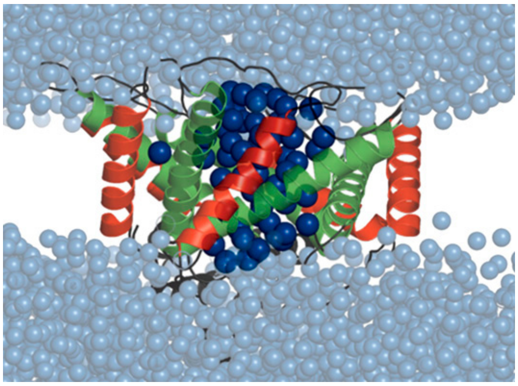

FIGURE 5 Water-permeable channel pore at the final expanded state ($t = 5$ μs) in V21D simulated at $T = 323$ K and $\gamma = 77$ mN/m. Highlighted are the water molecules within a 3-nm-diameter sphere. The diameter of the narrowest part of the pore equals 1.5 nm.

V21D and the WT at elevated temperature, an open and conducting state. Possibly, this open state is an intermediate one rather than the fully open. No clear definition of the fully open state of Tb-MscL or its mutants is available. Experimental estimations of the pore size are mainly indirect and based either on the Hille's model (46) relating the channel conductance to its geometry, or channel-mediated protein efflux experiments (47). However, such estimates are exclusively available for Eco-MscL and give a pore radius of the fully open state in the range 1–2 nm, somewhat larger that the maximum channel radius (0.7–0.75 nm) observed in this work.

CONCLUSION AND OUTLOOK

In summary, we have shown that the tension-induced gating of a membrane-embedded mechanosensitive channel (Tb-MscL) can be simulated using a novel coarse-grained protein model. Starting from the closed crystal structure, considerable opening of the channel is observed at a tension close to the rupture tension of the lipid bilayer. Simulations of the GOF mutant V21D reveal a lower gating tension in agreement with experimental data. After an irislike gating mechanism, an open state of the mutant is reached on a multi-microsecond timescale.

The study presented here opens up a number of ways to further deepen our understanding of the gating of mechanosensitive channels. First, the intermediate structures predicted along the gating pathway could be used as starting structures for fine-grained simulations. The importance of some of the atomic details left out in the CG models could thus be revealed. Second, the coarse-grained approach allows for a systematic exploration of the effect of lipid composition and protein mutations, which can be compared and further tested by experiments such as the measurements of gating tension as a function of membrane thickness (48). Computation of the lateral pressure profiles in connection to the gating thresholds would also allow for a direct test of theoretical models (49–51). In connection to this, the effect of curvature could be explored by embedding the channel into a small liposome. Pioneering efforts in this direction have been undertaken recently using all-atom models (52). With the CG model employed here, small liposomes can be modeled (53), allowing the full gating process to be simulated under realistic, i.e., hypoosmotic shock, conditions. Finally, multicopy simulations are nowadays feasible which will shed light on the cooperativity of the gating process, and reveal possible membrane-mediated protein-protein aggregation (as predicted recently from elastic models applied to MscL (54)).

We thank B. Poolman for reading the manuscript, thoughtful discussions, and valuable comments. We also thank J. Streutker and F. van Hoesel for help with the visualization of Fig. 2.

This work was carried out under the research program of the Zernike Institute for Advanced Materials.

REFERENCES

1. Hamill, O. P., and B. Martinac. 2001. Molecular basis of mechanotransduction in living cells. *Physiol. Rev.* 81:685–740.
2. Ajouz, B., C. Berrier, A. Garrigues, M. Besnard, and A. Ghazi. 1998. Release of thioredoxin via the mechanosensitive channel MscL during osmotic downshock of *Escherichia coli* cells. *J. Biol. Chem.* 273: 26670–26674.
3. Moe, P. C., G. Levin, and P. Blount. 2000. Correlating a protein structure with function of a bacterial mechanosensitive channel. *J. Biol. Chem.* 275:31121–31127.
4. Sukharev, S., P. Blount, B. Martinac, H. R. Guy, and C. Kung. 1996. MscL: a mechanosensitive channel in *Escherichia coli*. *Soc. Gen. Physiol. Ser.* 51:133–141.
5. Sukharev, S., M. Betanzos, C. S. Chiang, and H. R. Guy. 2001. The gating mechanism of the large mechanosensitive channel MscL. *Nature.* 409:720–724.
6. Perozo, E., D. M. Cortes, P. Sompornpisut, A. Kloda, and B. Martinac. 2002. Open channel structure of MscL and the gating mechanism of mechanosensitive channels. *Nature.* 418:942–948.
7. Moe, P., and P. Blount. 2005. Assessment of potential stimuli for mechano-dependent gating of MscL: effects of pressure, tension, and lipid headgroups. *Biochemistry.* 44:12239–12244.
8. Cruickshank, C. C., R. F. Minchin, A. C. Le Dain, and B. Martinac. 1997. Estimation of the pore size of the large-conductance mechanosensitive ion channel of *Escherichia coli*. *Biophys. J.* 73:1925–1931.
9. Sukharev, S. I., W. J. Sigurdson, C. Kung, and F. Sachs. 1999. Energetic and spatial parameters for gating of the bacterial large conductance mechanosensitive channel, MscL. *J. Gen. Physiol.* 113: 525–539.
10. Hase, C. C., A. C. Le Dain, and B. Martinac. 1995. Purification and functional reconstitution of the recombinant large mechanosensitive ion channel (MscL) of *Escherichia coli*. *J. Biol. Chem.* 270:18329–18334.
11. Maurer, J. A., D. E. Elmore, H. A. Lester, and D. A. Dougherty. 2000. Comparing and contrasting *Escherichia coli* and *Mycobacterium tuberculosis* mechanosensitive channels (MscL). New gain of function mutations in the loop region. *J. Biol. Chem.* 275:22238–22244.
12. Maurer, J. A., and D. A. Dougherty. 2001. A high-throughput screen for MscL channel activity and mutational phenotyping. *Biochim. Biophys. Acta.* 1514:165–169.
13. Chang, G., R. H. Spencer, A. T. Lee, M. T. Barclay, and D. C. Rees. 1998. Structure of the MscL homolog from *Mycobacterium tuberculosis*: a gated mechanosensitive ion channel. *Science.* 282:2220–2226.
14. Elmore, D. E., and D. A. Dougherty. 2001. Molecular dynamics simulations of wild-type and mutant forms of the *Mycobacterium tuberculosis* MscL channel. *Biophys. J.* 81:1345–1359.
15. Colombo, G., S. J. Marrink, and A. E. Mark. 2003. Simulation of MscL gating in a bilayer under stress. *Biophys. J.* 84:2331–2337.
16. Gullingsrud, J., D. Kosztin, and K. Schulten. 2001. Structural determinants of MscL gating studied by molecular dynamics simulations. *Biophys. J.* 80:2074–2081.
17. Gullingsrud, J., and K. Schulten. 2003. Gating of MscL studied by steered molecular dynamics. *Biophys. J.* 85:2087–2099.
18. Sukharev, S., S. R. Durell, and H. R. Guy. 2001. Structural models of the MscL gating mechanism. *Biophys. J.* 81:917–936.
19. Betanzos, M., C. S. Chiang, H. R. Guy, and S. Sukharev. 2002. Large iris-like expansion of a mechanosensitive channel protein induced by membrane tension. *Nat. Struct. Biol.* 9:704–710.
20. Kong, Y., Y. Shen, T. E. Warth, and J. Ma. 2002. Conformational pathways in the gating of *Escherichia coli* mechanosensitive channel. *Proc. Natl. Acad. Sci. USA.* 99:5999–6004.
21. Markin, V. S., and J. P. Albanesi. 2002. Membrane fusion: stalk model revisited. *Biophys. J.* 82:693–712.

22. Wiggins, P., and R. Phillips. 2004. Analytic models for mechanotransduction: gating a mechanosensitive channel. *Proc. Natl. Acad. Sci. USA*. 101:4071–4076.

23. Y. Tang, G. Coa, X. Chen, J. Yoo, A. Yething, and Q. Ciu. 2006. A finite element framework for studying the mechanical response of macromolecules: application to the gating of the mechanosensitive channel MscL. *Biophys. J*. 91:1248–1263.

24. Marrink, S. J., A. H. de Vries, and A. E. Mark. 2004. Coarse-grained model for semiquantitative lipid simulations. *J. Phys. Chem. B*. 108: 750–760.

25. Marrink, S. J., H. J. Risselada, S. Yefimov, D. P. Tieleman, and A. H. de Vries. 2007. The MARTINI forcefield: coarse-grained model for biomolecular simulations. *J. Phys. Chem. B*. 111:7812–7824.

26. Rand, R. P., and V. A. Parsegian. 1989. Hydration forces between phospholipid bilayers. *Biochim. Biophys. Acta*. 988:351–376.

27. Marrink, S. J., and A. E. Mark. 2004. Molecular view of hexagonal phase formation in phospholipid membranes. *Biophys. J*. 87:3894–3900.

28. Shih, A. Y., A. Arkhipov, P. L. Freddolino, and K. Schulten. 2006. Coarse-grained protein-lipid model with application to lipoprotein particles. *J. Phys. Chem. B*. 110:3674–3684.

29. Bond, P. J., and M. S. P. Sansom. 2006. Insertion and assembly of membrane proteins via simulation. *J. Am. Chem. Soc*. 128:2697–2704.

30. Periole, X., T. Huber, S. J. Marrink, and T. P. Sakmar. 2007. G protein-coupled receptors self-assemble in dynamics simulations of model bilayers. *J. Am. Chem. Soc*. 129:10126–10132.

31. Radzicka, A., and R. Wolfenden. 1988. Comparing the polarities of amino acids: side chain distribution coefficients between the vapor phase, cyclohexane, 1-octanol, and neutral aqueous solution. *Biochemistry*. 27: 1664–1670.

32. Wolfenden, R., L. Andersson, P. Cullis, and C. Southgate. 1981. Affinities of amino-acid side chains for solvent water. *Biochemistry*. 20:849–855.

33. Lindahl, E., B. Hess, and D. van der Spoel. 2001. GROMACS 3.0: a package for molecular simulation and trajectory analysis. *J. Mol. Model*. 7:306–317.

34. Smart, O. S., J. G. Neduvelil, X. Wang, B. A. Wallace, and M. S. P. Sansom. 1996. HOLE: a program for the analysis of the pore dimensions of ion channel structural models. *J. Mol. Graph*. 14:354–360.

35. Berendsen, H. J. C., J. P. M. Postma, W. F. van Gunsteren, A. DiNola, and J. R. Haak. 1984. Molecular dynamics with coupling to an external bath. *J. Chem. Phys*. 81:3684–3689.

36. White, S. H. 1980. Small phospholipid vesicles: internal pressure, surface tension, and surface free energy. *Proc. Natl. Acad. Sci. USA*. 77:4048–4050.

37. Oakley, A. J., B. Martinac, and M. C. Wilce. 1999. Structure and function of the bacterial mechanosensitive channel of large conductance. *Protein Sci*. 8:1915–1921.

38. Elmore, D. E., and D. A. Dougherty. 2003. Investigating lipid composition effects on the mechanosensitive channel of large conductance (MscL) using molecular dynamics simulations. *Biophys. J*. 85:1512–1524.

39. Zhelev, D. V., and D. Needham. 1993. Tension stabilized pores in giant vesicles: determination of pore size and pore line tension. *Biochim. Biophys. Acta*. 1147:89–104.

40. Evans, E., and V. Heinrich. 2003. Dynamic strength of fluid membranes. *Compte Rendus*. 4:265–274.

41. Leontiadou, H., A. E. Mark, and S. J. Marrink. 2004. Molecular dynamics simulations of hydrophilic pores in lipid bilayers. *Biophys. J*. 86:2156–2164.

42. Shapolov, G., R. Bass, D. C. Rees, and H. A. Lester. 2003. Open-state disulfide crosslinking between *Mycobacterium tuberculosis* mechanosensitive channel subunits. *Biophys. J*. 84:2357–2365.

43. Iscla, I., G. Levin, R. Wray, and P. Blount. 2007. Disulfide trapping the mechanosensitive MscL into a gating-transition state. *Biophys. J*. 92: 1224–1232.

44. Spencer, R. H., G. Chang, and D. C. Rees. 1999. Pulling the plug: structural insights on a gated mechanosensitive channel. *Curr. Opin. Struct. Biol*. 9:448–454.

45. Batiza, A. F., I. Rayment, and C. Kung. 1999. Channel gate! Tension, leak and disclosure. *Structure*. 7:99–103.

46. Hille, B. 1968. Charges and potentials at the nerve surface. Divalent ions and pH. *J. Gen. Physiol*. 51:199–219.

47. Van den Bogaart, G., V. Krasnikov, and B. Poolman. 2007. Dual-color fluorescence-burst analysis to probe protein efflux through the mechanosensitive channel MscL. *Biophys. J*. 92:1233–1240.

48. Perozo, E., A. Kloda, D. M. Cortes, and B. Martinac. 2002. Physical principles underlying the transduction of bilayer deformation forces during mechanosensitive channel gating. *Nat. Struct. Biol*. 9:696–703.

49. Cantor, R. S. 1999. Lipid composition and the lateral pressure profile in bilayers. *Biophys. J*. 76:2625–2639.

50. Gullingsrud, J., and K. Schulten. 2004. Lipid bilayer pressure profiles and mechanosensitive channel gating. *Biophys. J*. 86:3496–3509.

51. Niemela, P. S., S. Ollila, M. T. Hyvonen, M. Karttunen, and I. Vattulainen. 2007. Assessing the nature of lipid raft membranes. *PLOS Comp. Biol*. 3:304–312.

52. Meyer, G. R., J. Gullingsrud, K. Schulten, and B. Martinac. 2006. Molecular dynamics study of MscL interactions with a curved lipid bilayer. *Biophys. J*. 91:1630–1637.

53. Marrink, S. J., and A. E. Mark. 2003. Molecular dynamics simulation of the formation, structure, and dynamics of small phospholipid vesicles. *J. Am. Chem. Soc*. 125:15233–15242.

54. Ursell, T., K. C. Huang, E. Peterson, and R. Phillips. 2007. Cooperative and spatial organization of membrane proteins through elastic interactions. *PLOS Comp. Biol*. 3:803–812.